ACS APPLIED MATERIALS & INTERFACES

Research Article

www.acsami.org

Air Stable Organic Salt As an n-Type Dopant for Efficient and Stable Organic Light-Emitting Diodes

Zhengyang Bin, Lian Duan,* and Yong Qiu

Key Lab of Organic Optoelectronics & Molecular Engineering, Department of Chemistry, Tsinghua University, Beijing, 100084, People's Republic of China

Supporting Information

ABSTRACT: Air-stable and low-temperature-evaporable n-type dopants are highly desired for efficient and stable organic light-emitting diodes (OLEDs). In this work, 2-(2-Methoxyphenyl)-1,3-dimethyl-1H-benzoimidazol-3-ium iodide (*o*-MeO-DMBI-I), a thermally decomposable precursor of organic radical *o*-MeO-DMBI, has been employed as a novel n-type dopant in OLEDs, because of its air stability, low decomposition temperature, and lack of atom diffusion. The n-type electrical doping is evidenced by the rapid increase in current density of electron-only devices and the large improvement in conductivity, originated from increased electron concentration in electron-transport layer (ETL) and reduced electron injection barrier. A highly efficient and stable OLED is created using *o*-MeO-DMBI as an n-type dopant in Bphen. Compared with the control device with its high-temperature-evaporable n-type dopant cesium carbonate (Cs_2CO_3), *o*-MeO-DMBI-doped device showed an incredible boom in current efficiency from 28.6 to 42.2 cd/A. Moreover, the lifetime ($T_{70\%}$) of *o*-MeO-DMBI-doped device is 45 h, more than 20 times longer than that of the Cs_2CO_3-doped device (2 h). The enhanced efficiency and stability are attributed to the improved balance of holes and electrons in the emissive layer, and the eliminated atom diffusion of cesium.

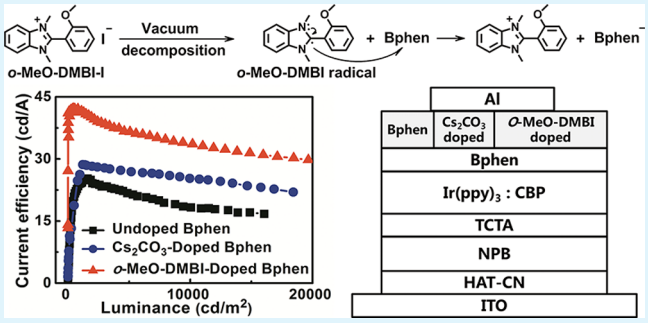

KEYWORDS: *n-type dopant, organic salt, organic radical, high efficiency, organic light-emitting diodes*

1. INTRODUCTION

Organic light-emitting diodes (OLEDs) have triggered a great deal of research on organic semiconductors (OSCs) and devices due to their potential application as flat-panel displays and solid-state illumination for its high power efficiency, low weight, and flexibility.[1] Although significant progress has been made in vacuum-deposited OLEDs, low driving voltage remains a crucial requirement to improve the power efficiency and reduce the power consumption of OLEDs.[2] The p-type and n-type doping in charge transport layers are the most well-known methods to reduce operation voltage in devices owing to the increased conductivity. Currently, a wide range of materials have been adopted as effective p-type dopants in hole transporting materials.[3,4] In contrast to p-type doping, n-type doping is intrinsically more difficult for the requirement of extremely high highest occupied molecular orbital (HOMO) molecules, which are chemically very reactive and easily oxidized in the presence of ambient oxygen and water.[5] The alkali metals, such as lithium (Li)[6] and cesium (Cs),[7] have been extensively studied and once widely used as n-type dopants in OLEDs. However, high reactivity and diffusivity severely restrict the wide application of these dopants.[8] Alkali salts, such as cesium azide (CsN_3)[9] and cesium carbonate (Cs_2CO_3),[10] are anticipated to be more air stable with respect to high reactivity, but still do not avoid the problem of atom diffusion, resulting in severe exciton quenching in the emitting layer.[11] Moreover, inorganic dopants which are based on alkaline metal derivatives only decompose at temperatures that are much higher than the normal evaporation temperature of organic elecrtron transporting materials (ETMs). The coevaporation in the organic chamber will result in outgassing of organic materials from the chamber wall during evaporation because of the high heating temperature.[9] Thus, organic n-type dopants with low deposition temperatures come into researchers' view. Leo's group reported many precursor n-type dopants, such as pyronine B[12] and crystal violet,[13] and Bao's group also reported a series of organic n-type dopants based on the benzimidazole sturcture, such as *o*-MeO-DMBI-I[14] and derivatives of the DMBI molecule.[15,16] These dopants all showed excellent doping abilities in C_{60} and 7,7,8,8-tetracyanoquinodimethane (TCNQ), which are both widely used ETMs in organic thin-film translators (OTFTs) or solar cells.[14−16] But organic n-type dopants have rarely been used in OLEDs. Organic n-type dopant could not only have a great advantage of low decomposition temperature, but which is more beneficial for OLEDs compared with solar cells or

Received: September 20, 2014
Accepted: March 13, 2015
Published: March 13, 2015

DOI: 10.1021/acsami.5b00839
ACS Appl. Mater. Interfaces 2015, 7, 6444−6450

OTFTs, it could avoid the problem of atom diffusion, thus achieving a higher quantum efficiency and a longer lifetime.

In this work, we present an organic salt, *o*-MeO-DMBI-I, as a precursor of n-type dopant in OLEDs. *o*-MeO-DMBI-I, shown in Figure 1, which is stable in air, is deduced to decompose to its neutral radical *o*-MeO-DMBI during vacuum heating. *o*-MeO-DMBI may undergo an electron transfer to Bphen, leading to an increase in electron concentration and electron mobility. *o*-MeO-DMBI was utilized in OLEDs to replace the traditionally used high-temperature-evaporable n-type dopant of Cs_2CO_3, which is known to release Cs with a strong diffusion tendency in organic materials. A highly efficient and stable OLED was created using *o*-MeO-DMBI-doped Bphen as an ETL, due to an eliminated atom diffusion by Cs, an improved transport property of Bphen, and a reduced electron injection barrier.

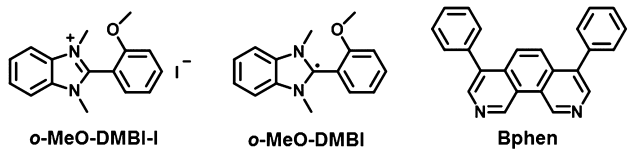

Figure 1. Molecular structures of the organic materials used in this work.

2. EXPERIMENTAL SECTION

2.1. Device Fabrication. *o*-MeO-DMBI-I was synthesized as reported previously,[14] and Bphen was purchased from Jilin Optical and Electronic Materials Company, which were purified by repeated temperature-gradient vacuum sublimation and received with a purity of more than 99.5%. Thus, it was used directly without further purification. All the films were prepared by conventional thermal deposition inside a high vacuum chamber at 10^{-4} Pa. A quartz crystal sensor monitored the thickness of organic layers in situ. All devices were fabricated on ITO substrates with sheet resistances about 15 Ω/□ after UV-ozone treatments. After vacuum deposition, the devices were transferred to a glovebox filled with nitrogen without being exposed to air and then encapsulated with glass plates. All device measurements were done after being encapsulated.

2.2. Measurement. Atom concentration of iodine in *o*-MeO-DMBI-doped Bphen film was characterized by X-ray photoelectron spectroscopy (XPS, ULVAC-PHI, PHI Quantera SXM). The crystallinities of undoped and *o*-MeO-DMBI-doped Bphen films on glass substrates were determined by X-ray diffraction (XRD, D/max-IIIA 3KW, Cu-Ka). Absorption spectra were recorded with an UV−vis spectrophotometer (Jobin Yvon, FluoroMax-3). The current density−luminance−voltage characteristics were measured by a Keithley 4200 semiconductor characterization system. Mobilities were determined by time-of-flight (TOF) method. The flight time t_T, which is the time that carriers pass through organic layer, was derived from the intersection of the two straight lines in the double-logarithmic plot of the transient photocurrent. And mobility can be described as L^2/t_TV, where L is the film thickness, and V is the applied voltage.[17−19] The resistances R of the TOF devices were measured by Agilent 4294A. Then the conductivity σ, which is equal to reciprocal of the electrical resistivity ρ in the same device, could be described as l/RS, where, l is the thickness of organic layer, and S is the area contacted with cathode directly.

3. RESULTS AND DISCUSSION

3.1. Thermal Properties of *o*-MeO-DMBI-I. Thermal gravity analysis (TGA) was used to study the thermal properties of *o*-MeO-DMBI-I. As can be seen in Figure 2, *o*-MeO-DMBI-I started to decompose at about 240 °C, which is much lower than the evaporation temperature of traditionally used inorganic n-type dopants, and beneficial for coevaporating with low-temperature-evaporable organic ETMs.

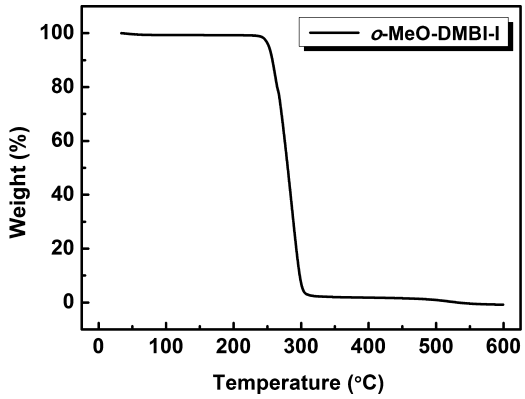

Figure 2. TGA curve of *o*-MeO-DMBI-I.

3.2. Doping Mechanism of *o*-MeO-DMBI-I and Bphen. To study the doping mechanism of *o*-MeO-DMBI-I and Bphen, the absorbance spectra were measured, as shown in Figure 3. For solution-processed *o*-MeO-DMBI-I film, there was no significant absorption between 350 and 600 nm. After vacuum deposition, a new band with a maximum absorption at 385 nm began to form, which indicated that a new product was formed and deposited in the film. But when *o*-MeO-DMBI-I was deposited in Bphen, the absorption peak at 385 nm disappeared, confirming that the molecule formed during vacuum deposition transformed back to its previous cationic state. Thus, we can get that the new molecule formed through vacuum deposition was quite reactive and it could react with Bphen fast, transformed back to its previous cationic state upon oxidation process. Consequently, the cation could be stabilized by the adjacent electron-rich phenyl ring and two nitrogen atoms, making this electron-transfer process irreversible and a stable n-type doping could be realized.

To exclude the doping mechanism further, XPS measurement was performed on the doped Bphen film, as shown in Figure 4. By carefully examining the XPS spectrum, no iodide peak was observed in the film, indicating that *o*-MeO-DMBI-I was reduced and lost I^-, and there was no risk of iodide contamination by this precursor approach. Hence, it is the radical *o*-MeO-DMBI that acted as an n-type dopant in Bphen, but not its precursor molecule *o*-MeO-DMBI-I.

Here, the doping mechanism is proposed as shown in Figure 5. *o*-MeO-DMBI-I is not a strong electron donor and could not donate electrons to Bphen directly. But when it was heated, it could decompose to its neutral radical, namely *o*-MeO-DMBI, upon heating. Then *o*-MeO-DMBI, with a high HOMO of −2.53 eV according to B3LYP/6-31G* calculations using Gaussian 03,[14] might undergo an electron transfer to BPhen, which has a lowest unoccupied molecular orbital (LUMO) of 2.8 eV.[2] In results, *o*-MeO-DMBI$^+$ was formed again and Bphen was reduced. Moreover, the *o*-MeO-DMBI$^+$ formed after doping do not have any self-absorption, good for color stability of OLEDs.

3.3. Quantum Chemical Calculations. As is well-known in thermodynamics, the feasibility and spontaneity of a reaction can be evaluated by the Gibbs free energy $[\Delta_rG_m(T,p)]$ of the reaction, thus to further evaluate the reaction between *o*-MeO-DMBI and Bphen, the Gibbs free energy was calculated from Quantum Chemical Calculations. All our calculations were performed by using the Gaussian 03 software package.[20] The

DOI: 10.1021/acsami.5b00839
ACS Appl. Mater. Interfaces 2015, 7, 6444−6450

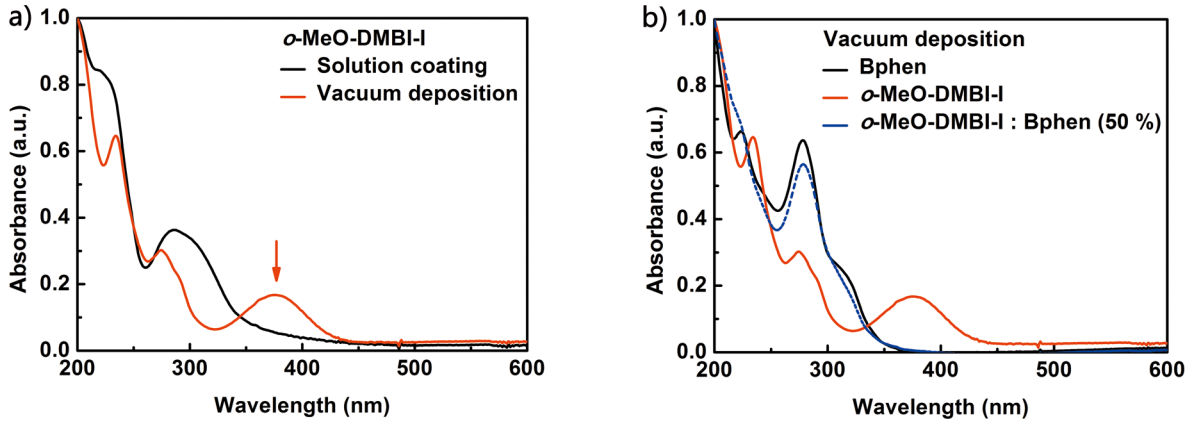

Figure 3. (a) The absorbance spectra of *o*-MeO-DMBI-I films by vacuum deposition or by evaporating the solvent of a CH_2Cl_2 solution. (b) The absorbance spectra of Bphen, *o*-MeO-DMBI-I and doped Bphen films by vacuum deposition.

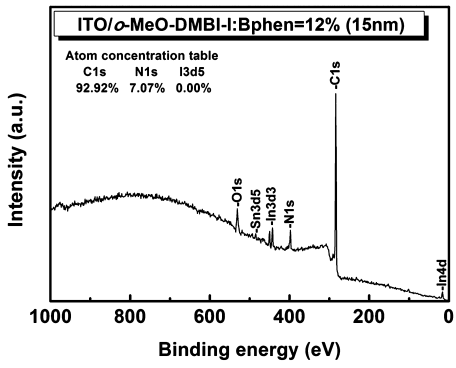

Figure 4. XRD spectrum of the doped Bphen film.

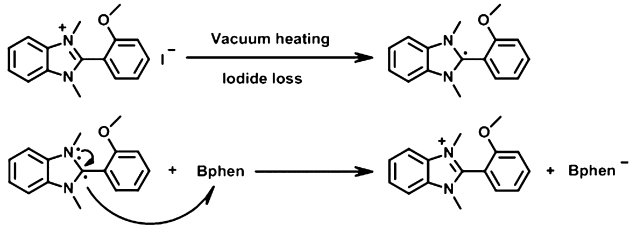

Figure 5. Proposed doping mechanism of *o*-MeO-DMBI-I and ETM.

B3LYP density functional was selected to calculate the Gibbs free energy for each molecule, radical and charged species. The standard 6-31+G(d) basis set was used for the geometry optimizations and frequency calculations, while the single-point energy calculations were performed with the 6-311++G(2df,2p) basis set. The Gibbs free energy of each species was calculated using the B3LYP/6-311++G(2df,2p) electronic energy and the zero-point vibrational energy and thermal corrections (0 f 298 K) obtained at the B3LYP/6-31+G(d) level.[21]

Here, we take the assumption that the reaction takes place at a constant temperature of 298.15 K and pressure of 1.0 atm owing to the extremely short reaction time in the encapsulated devices. A negative Δ_rG_m of −393.83 kJ/mol was calculated for this reaction, summarized in Table 1. Thus, it is thermodynamically reasonable for the reaction between *o*-MeO-DMBI and Bphen.

3.4. Doping Effects of *o*-MeO-DMBI as an n-Type Dopant in Bphen. The current−voltage characteristics of the electron-only devices were used to evaluate the transporting and injection properties of *o*-MeO-DMBI-doped Bphen film.

Table 1. Calculation of the Gibbs Free Energy for the Reaction

Reaction: *o*-MeO-DMBI + Bphen → *o*-MeO-DMBI$^+$ + Bphen$^-$				
	o-MeO-DMBI	Bphen	*o*-MeO-DMBI$^+$	Bphen$^-$
Gibbs free energy	−804.63	−1033.49	−804.47	−1033.78
Δ_rG_m	−0.15 (a.u.) = −393.83 (kJ/mol)			

The structures of electron-only devices are shown in Table 2, and the performances are summarized in Figure 6.

Table 2. Structures of Electron Only Devices

device	structures
A	ITO/BCP (10 nm)/Bphen (100 nm)/Al
B	ITO/BCP (10 nm)/*o*-MeO-DMBI:Bphen (*x* %, 100 nm)/Al
C	ITO/BCP (10 nm)/*o*-MeO-DMBI/:Bphen (*x* %, 95 nm)/Bphen (5 nm)/Al

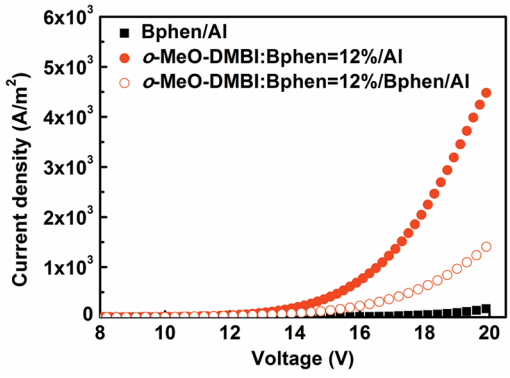

Figure 6. Current density−voltage characteristics of electron-only devices.

In these devices, BCP stands for 2,9-dimethyl-4,7-diphenyl-1,10-phenanthroline and was used as a blocking layer. The optimized doping concentration was 12%, (see Supporting Information, SI, Figure S1), at a higher doping concentration of 16%, the current density decreased rapidly due to the tendency of *o*-MeO-DMBI to aggregate and the localization of the donated electrons around the dopant molecule in the film.[14,22,23] Compared with undoped device A, device C showed an improvement in the current density from 4.6 to

DOI: 10.1021/acsami.5b00839
ACS Appl. Mater. Interfaces 2015, 7, 6444−6450

61.2 A/m^2 at a 18 V bias, originated from highly efficient n-doping of *o*-MeO-DMBI with Bphen. When *o*-MeO-DMBI-doped Bphen layer was adopted as an electron injection layer to contact with cathode directly, a higher current density of 214.4 A/m^2 at the same bias was achieved, demonstrating a lowed interfacial energy barrier was formed between Bphen and Al upon n-doping by *o*-MeO-DMBI. Thus, *o*-MeO-DMBI is a good n-type dopant in Bphen, because it could not only improve the transport property of Bphen, but also lower the interfacial energy barrier between Bphen and cathode.

TOF measurements were performed to investigate the doping effect of *o*-MeO-DMBI in Bphen. The structures of the TOF samples were ITO/Bphen/Ag, and ITO/*o*-MeO-DMBI:Bphen = 12%/Ag, where the thickness of organic layer is 0.8 μm. Figure 7 shows the electron mobilities of undoped

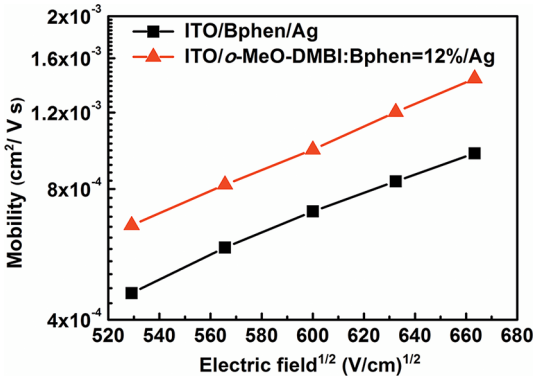

Figure 7. Electron mobilities of undoped and *o*-MeO-DMBI-doped Bphen films under various fields at room temperature.

Bphen and *o*-MeO-DMBI-doped Bphen films. Mobilities of undoped Bphen films were in the range from (4−9) × 10^{-4} cm^2 V^{-1} s^{-1} and exhibited positive correlations with electric fields, which agrees well with the values reported earlier.[24] In the case of *o*-MeO-DMBI-doped Bphen device, electron mobilities showed a slight increase and also exhibited positive correlations with electric fields, which means the position disorder of Bphen molecules were not changed a lot in the doped films.[25,26]

Because Bphen molecule is easy to crystallize and crystallization has a big effect on mobility, XRD patterns were measured to study the variation in crystallization for undoped and *o*-MeO-DMBI-doped Bphen films. As depicted in Figure 8, both films were amorphous, and no additional peaks could be seen before and after *o*-MeO-DMBI was introduced. Thus, the same crystallinity conditions of the two films wiped out the influence of crystallinity to mobility improvement, leaving the charge transfer and trap filling to be the dominant factor on mobility.[27]

Moreover, upon doping, the film conductivity was also increased from 3.8 × 10^{-7} to 1.2 × 10^{-6} S/cm^{-1}, more than 3 times larger than undoped Bphen film. Using the eq (1) $\sigma = en\mu$, where σ is conductivity, e is equal to 1.60 × 10^{-19} C, and μ is electron mobility, which was chose at an electric field of 5.0 × 10^4 V cm^{-1}, electron concentrations (n) of both doped and undoped films were deduced, and summarized in Table 3.[28] The electron concentrations showed an increase from 4.1 × 10^{15} to 9.5 × 10^{15} cm^{-3} upon doping, originated from charge transfer of *o*-MeO-DMBI to Bphen molecule.

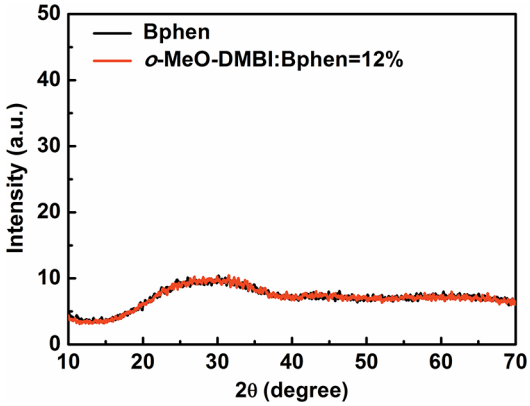

Figure 8. XRD patterns of undoped and *o*-MeO-DMBI-doped Bphen films.

Table 3. Mobilities, Conductivities, and Electron Concentrations of Both Doped and Undoped Bphen Films

	undoped Bphen	12% doped Bphen
mobility (cm^2 V^{-1} s^{-1})	5.9 × 10^{-4}	8.2 × 10^{-4}
conductivity (S cm^{-1})	3.8 × 10^{-7}	1.20 × 10^{-6}
electron concentration (cm^{-3})	4.1 × 10^{15}	9.5 × 10^{15}

3.5. Phosphorescent OLEDs. Finally, *o*-MeO-DMBI-doped Bphen film was applied to phosphorescent OLEDs. In order to evaluate the doping effect of *o*-MeO-DMBI further, Cs_2CO_3, a widely used n-type dopant,[10] was also used to dope with Bphen. The optimized doping concentration was 12% for *o*-MeO-DMBI-doped Bphen, while 10% for Cs_2CO_3-doped Bphen, (see SI Figures S2 and S3). The device structures are ITO/HAT-CN (5 nm)/NPB (40 nm)/Ir(ppy)$_3$:CBP (10%, 30 nm)/Bphen (10 nm)/undoped, 10%Cs_2CO_3-doped, or 12%*o*-MeO-DMBI-doped Bphen (30 nm)/Al, where HAT-CN stands for 1,4,5,8,9,11-hexaazatriphenylene hexacarbonitrile, NPB stands for *N*,*N*′-di(naphthalene-1-yl)-*N*,*N*′-diphenyl-benzidine, Ir(ppy)$_3$ stands for tris(2-phenylpyridine) iridium, and CBP stands for 4,4-*N*,*N*-dicarbazolylbiphenyl.

Figure 9 compares the device performances of the three devices. Doped with *o*-MeO-DMBI, a remarkable increase in the current density was achieved, and the luminance was significantly increased from 2.3 × 10^2 to 1.3 × 10^5 cd/m^2 at a 8 V bias, an increase by more than 2 orders of magnitude. The turn on voltage was also largely decreased, and low driving voltage could lead to improve the power efficiency and reduce the power consumption of OLEDs.[2] Compared with the control device with high-temperature-evaporable n-type dopant cesium carbonate (Cs_2CO_3), the *o*-MeO-DMBI-doped device showed an incredible boom in current efficiency from 28.6 to 42.2 cd/A. Because phosphorescent OLEDs are very sensitive to the exciton behavior in the emitting layer, the lower current efficiency of Cs_2CO_3-doped device should be blamed mainly for the atom diffusion of diffused Cs, and thus severely exciton quenching in the emitting layer.

The exciton quenching by diffused Cs can be proven by photoluminescence (PL) measurements, as shown in Figure 10. The structures of the films are SiO_2/Ir(ppy)$_3$:CBP (10%, 30 nm)/Bphen (10 nm)/undoped, 10%Cs_2CO_3-doped, or 12%*o*-MeO-DMBI-doped Bphen (30 nm). The PL intensity of undoped and 12% *o*-MeO-DMBI-doped films were almost the same, while the PL intensity of 10% Cs_2CO_3-doped film was

DOI: 10.1021/acsami.5b00839
ACS Appl. Mater. Interfaces 2015, 7, 6444−6450

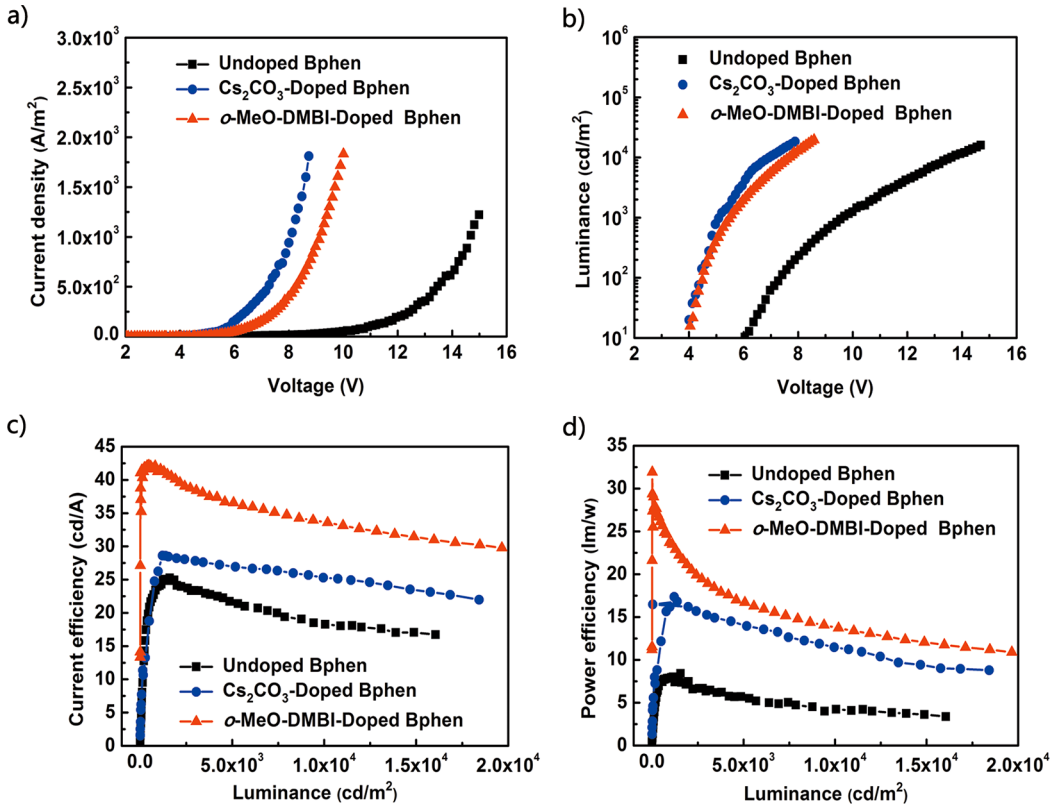

Figure 9. (a) Current density–voltage, (b) luminance–voltage, (c) current efficiency–luminance, and (d) power efficiency–luminance characteristics of undoped, Cs_2CO_3-doped, and *o*-MeO-DMBI-doped devices.

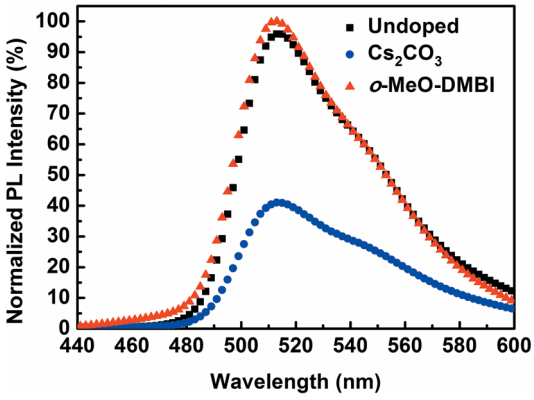

Figure 10. PL spetra of undoped, Cs_2CO_3-doped, and *o*-MeO-DMBI-doped films.

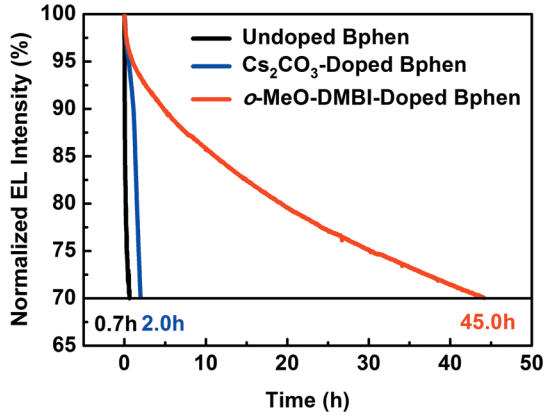

Figure 11. Luminance–deterioration curves of undoped and doped devices.

only 40% of that in the *o*-MeO-DMBI-doped film, indicating a severe exciton quenching by diffused Cs.

The exciton quenching by diffused Cs could also be approved by luminance decay with time. $T_{70\%}$, defined as the time when the actual luminance decays to 70% of the initial luminance of 1000 cd/m^2 at a room temperature, was measured to compare the stability of doped and undoped devices. As can be seen from Figure 11, $T_{70\%}$ of OLEDs with undoped, Cs_2CO_3-doped and *o*-MeO-DMBI-doped ETLs are 0.7, 2.0, and 45.0 h, respectively, corresponding to 3 times and 65 times improvement in the device lifetime. The prolonged lifetime is mainly attributed to the eliminated atom diffusion by Cs, and also attributed to an improved transport property in the ETL and a reduced electron injection barrier, thus the better balance of holes and electrons in the emissive layer.[26,29]

4. CONCLUSIONS

In summary, *o*-MeO-DMBI-I, an air-stable and low-temperature-evaporable organic salt, was first employed as an precursor molecule for an n-type dopant in OLEDs. The current density of electron-only device has been largely advanced through the use of *o*-MeO-DMBI as an n-type dopant in Bphen. Upon doping, electron mobility and electron concentration both showed a rapid increase, leading to a great improvement of film conductivity. The improvement in the electron transporting property of ETM is attributed to the oxidation process due to the decomposition of *o*-MeO-DMBI-I to its neutral radical and then undergoes an electron transfer to Bphen host. When *o*-MeO-DMBI-doped Bphen was used as an

DOI: 10.1021/acsami.5b00839
ACS Appl. Mater. Interfaces 2015, 7, 6444–6450

ETL in phosphorescent OLEDs, a significant improvement in current density, efficiency, and lifetime were realized. Compared to the control device with high-temperature-evaporable n-type dopant of Cs_2CO_3, *o*-MeO-DMBI showed a similar n-doping ability, but no tendency of atom diffusion. Thus exciton quenching by metal atoms was eliminated, which is good for improving the current efficiency and stability.

To summarize, *o*-MeO-DMBI is an effective n-type dopant, which could not only avoid the problem of atom diffusion and high evaporation temperature, but also have a good n-doping ability as traditionally used inorganic n-type dopant.

It is the first work to employ an air stable organic salt as an n-type dopant in OLEDs, and the same concept may be further studied with careful molecular design, so as to replace the traditional used inorganic n-type dopants and promote the practical use of organic n-type dopants.

■ ASSOCIATED CONTENT

Supporting Information

Current density−voltage characteristics of electron-only devices with various *o*-MeO-DMBI doping concentrations. Current density−voltage, luminance−voltage, current efficiency−luminance, and power efficiency−luminance characteristics of Cs_2CO_3-doped and *o*-MeO-DMBI-doped devices with various doping concentrations. This material is available free of charge via the Internet at http://pubs.acs.org.

■ AUTHOR INFORMATION

Corresponding Author

*Tel: (008610) 62779988; fax: (008610) 62795137; e-mail: duanl@mail.tsinghua.edu.cn.

Notes

The authors declare no competing financial interest.

■ ACKNOWLEDGMENTS

We would like to thank the National Natural Science Foundation of China (Grant Nos. 51173096 and 21161160447) and the National Key Basic Research and Development Program of China (Grant No. 2015CB655002) for financial support.

■ REFERENCES

(1) Tang, C. W.; VanSlyke, S. A. Organic Electroluminescent Diodes. *Appl. Phys. Lett.* **1987**, *51*, 913−915.

(2) Yook, K. S.; Jeon, S. O.; Min, S.-Y.; Lee, J. Y.; Yang, H.-J.; Noh, T.; Kang, S.-K.; Lee, T.-W. Highly Efficient p-i-n and Tandem Organic Light-Emitting Devices Using an Air-Stable and Low-Temperature-Evaporable Metal Azide as an n-Dopant. *Adv. Funct. Mater.* **2010**, *20*, 1797−1802.

(3) Zhou, X.; Blochwitz, J.; Pfeiffer, M.; Nollau, A.; Fritz, T.; Leo, K. Enhanced Hole Injection into Amorphous Hole-Transport Layers of Organic Light-Emitting Diodes Using Controlled p-Type Doping. *Adv. Funct. Mater.* **2001**, *11*, 310−314.

(4) Greiner, M. T.; Helander, M. G.; Tang, W.-M.; Wang, Z.-B.; Qiu, J.; Lu, Z.-H. Universal Energy-Level Alignment of Molecules on Metal Oxides. *Nat. Mater.* **2012**, *11*, 76−81.

(5) Zhou, Y.; Fuentes-Hernandez, C.; Shim, J.; Meyer, J.; Giordano, A. J.; Li, H.; Winget, P.; Papadopoulos, T.; Cheun, H.; Kim, J.; Fenoll, M.; Dindar, A.; Haske, W.; Najafabadi, E.; Khan, T. M.; Sojoudi, H.; Barlow, S.; Graham, S.; Brédas, J.-L.; Marder, S. R.; Kahn, A.; Kippelen, B. A Universal Method to Produce Low−Work Function Electrodes for Organic Electronics. *Science.* **2012**, *336*, 327−332.

(6) Parthasarathy, G.; Shen, C.; Kahn, A.; Forrest, S. R. Lithium Doping of Semiconducting Organic Charge Transport Materials. *J. Appl. Phys.* **2001**, *89*, 4986−4992.

(7) Lee, J.-H.; Wu, M.-H.; Chao, C.-C.; Chen, H.-L.; Leung, M.-K. High Efficiency and Long Lifetime OLED Based on a Metal-Doped Electron Transport Layer. *Chem. Phys. Lett.* **2005**, *416*, 234−237.

(8) Naab, B. D.; Zhang, S.; Vandewal, K.; Salleo, A.; Barlow, S.; Marder, S. R.; Bao, Z. Effective Solution- and Vacuum-Processed n-Doping by Dimers of Benzimidazoline Radicals. *Adv. Mater.* **2014**, *26*, 4268−4272.

(9) Yook, K. S.; Jeon, S. O.; Min, S. Y.; Lee, J. Y.; Yang, H. J.; Noh, T.; Kang, S. K.; Lee, T. W. Highly Efficient p-i-n and Tandem Organic Light-Emitting Devices Using an Air-Stable and Low-Temperature-Evaporable Metal Azide as an n-Dopant. *Adv. Funct. Mater.* **2010**, *20*, 1797−1802.

(10) Lee, T.-W.; Noh, T.; Choi, B.-K.; Kim, M.-S.; Shin, D. W.; Kido, J. High-Efficiency Stacked White Organic Light-Emitting Diodes. *Appl. Phys. Lett.* **2008**, *92*, 043301−043301−3.

(11) Chan, C. K.; Kim, E. G.; Brédas, J. L.; Kahn, A. Molecular n-Type Doping of 1,4,5,8-Naphthalene Tetracarboxylic Dianhydride by Pyronin B Studied Using Direct and Inverse Photoelectron Spectroscopies. *Adv. Funct. Mater.* **2006**, *16*, 831−837.

(12) Werner, A.; Li, F.; Harada, K.; Pfeiffer, M.; Fritz, T.; Leo, K.; Machill, S. n-Type Doping of Organic Thin Films Using Cationic Dyes. *Adv. Funct. Mater.* **2004**, *14*, 255−260.

(13) Li, F.; Werner, A.; Pfeiffer, M.; Leo, K.; Liu, X. Leuco Crystal Violet as a Dopant for n-Doping of Organic Thin Films of Fullerene C60. *J. Phys. Chem. B* **2004**, *108*, 17076−17082.

(14) Wei, P.; Menke, T.; Naab, B. D.; Leo, K.; Riede, M.; Bao, Z. 2-(2-Methoxyphenyl)-1,3-dimethyl-1H-benzoimidazol-3-ium Iodide as a New Air-Stable n-Type Dopant for Vacuum-Processed Organic Semiconductor Thin Films. *J. Am. Chem. Soc.* **2012**, *134*, 3999−4002.

(15) Naab, B. D.; Guo, S.; Olthof, S.; Evans, E. G. B.; Wei, P.; Millhauser, G. L.; Kahn, A.; Barlow, S.; Marder, S. R.; Bao, Z. Mechanistic Study on the Solution-Phase n-Doping of 1,3-Dimethyl-2-aryl-2,3-dihydro-1H-benzoimidazole Derivatives. *J. Am. Chem. Soc.* **2013**, *135*, 15018−15025.

(16) Wei, P.; Liu, N.; Lee, H. R.; Adijanto, E.; Ci, L.; Naab, B. D.; Zhong, J. Q.; Park, J.; Chen, W.; Cui, Y.; Bao, Z. Tuning the Dirac Point in CVD-Grown Graphene through Solution Processed n-Type Doping with 2-(2-Methoxyphenyl)-1,3-dimethyl-2,3-dihydro-1H-benzoimidazole. *Nano Lett.* **2013**, *13*, 1890−1897.

(17) Li, C.; Duan, L.; Sun, Y.; Li, H.; Qiu, Y. Charge Transport in Mixed Organic Disorder Semiconductors: Trapping, Scattering, and Effective Energetic Disorder. *J. Phys. Chem. C* **2012**, *116*, 19748−19754.

(18) Bassler, H. Charge Transport in Disordered Orgainc Photoconductors—A Monte-Carlo Simulation Study. *Phys. Status Solidi B* **1993**, *175*, 15−56.

(19) Scher, H.; Montroll, E. W. Anomalous Transit-Time Dispersion in Amorphous Solids. *Phys. Rev. B* **1975**, *12*, 2455−2477.

(20) Frisch, M. J.; Trucks, G. W.; Schelegel, H. B.; Scuseria, G. E.; Robb, M. A.; Cheeseman, J. R.; Scalmani, G.; Barone, V.; Mennucci, B.; Petersson, G. A.; Nakatsuji, H.; Caricato, M.; Li, X.; Hratchian, H. P.; Izmaylov, A. F.; Bloino, J.; Zheng, G.; Sonnenberg, J. L.; Hada, M.; Ehara, M.; Toyota, K.; Fukuda, R.; Hasegawa, J.; Ishida, M.; Nakajima, T.; Honda, Y.; Kitao, O.; Nakai, H.; Vreven, T.; Montgomery, J. A., Jr.; Peralta, J. E.; Ogliaro, F.; Bearpark, M.; Heyd, J. J.; Brothers, E.; Kudin, K. N.; Staroverov, V. N.; Kobayashi, R.; Normand, J.; Raghavachari, K.; Rendell, A.; Burant, J. C.; Iyengar, S. S.; Tomasi, J.; Cossi, M.; Rega, N.; Millam, J. M.; Klene, M.; Knox, J. E.; Cross, J. B.; Bakken, V.; Adamo, C.; Jaramillo, J.; Gomperts, R.; Stratmann, R. E.; Yazyev, O.; Austin, A. J.; Cammi, R.; Pomelli, C.; Ochterski, J. W.; Morokuma, R. L. K.; Zakrzewski, V. G.; Voth, G. A.; Salvador, P.; Dannenberg, J. J.; Dapprich, S.; Daniels, A. D.; Farkas, O.; Foresman, J. B.; Ortiz, J. V.; Cioslowski, J.; Fox, D. J. *Gaussian 03*, revision B.05.; Gaussian Inc.: Wallingford, CT, 2004.

(21) Fu, Y.; Liu, L.; Yu, H.-Z.; Wang, Y.-M.; Guo, Q.-X. Quantum-Chemical Predictions of Absolute Standard Redox Potentials of

DOI: 10.1021/acsami.5b00839
ACS Appl. Mater. Interfaces 2015, 7, 6444−6450

Diverse Organic Molecules and Free Radicals in Acetonitrile. *J. Am. Chem. Soc.* **2005**, *127*, 7227−7234.
(22) Ha, S. D.; Kahn, A. Isolated Molecular Dopants in Pentacene Observed by Scanning Tunneling Microscopy. *Phys. Rev. B* **2009**, *80*, 195410.
(23) Maennig, B.; Pfeiffer, M.; Nollau, A.; Zhou, X.; Leo, K.; Simon, P. Controlled p-Type Doping of Polycrystalline and Amorphous Organic Layers: Self-Consistent Description of Conductivity and Field-Effect Mobility by a Microscopic Percolation Model. *Phys. Rev. B* **2001**, *64*, 195208.
(24) Naka, S.; Okada, H.; Onnagawa, H.; Tsutsui, T. High Electron Mobility in Bathophenanthroline. *Appl. Phys. Lett.* **2000**, *76*, 197−199.
(25) Borsenberger, P. M.; Pautmeier, L.; Bässler, H. Charge Transport in Disordered Molecular Solids. *J. Chem. Phys.* **1991**, *94*, 5447−5454.
(26) Bin, Z.; Duan, L.; Li, C.; Zhang, D.; Dong, G.; Wang, L.; Qiu, Y. Bismuth Trifluoride as a Low-Temperature-Evaporable Insulating Dopant for Efficient and Stable Organic Light-Emitting Diodes. *Org. Electron.* **2014**, *15*, 2439−2447.
(27) Jia, Y.; Duan, L.; Zhang, D.; Qiao, J.; Dong, G.; Wang, L.; Qiu, Y. Low-Temperature Evaporable Re_2O_7: An Efficient p-Dopant for OLEDs. *J. Phys. Chem. C* **2013**, *117*, 13763−13769.
(28) Zhang, Q.; Sun, Y.; Xu, W.; Zhu, D. Organic Thermoelectric Materials: Emerging Green Energy Materials Converting Heat to Electricity Directly and Efficiently. *Adv. Mater.* **2014**, *26*, 6829−6851.
(29) Aziz, H.; Popovic, Z. D. Degradation Phenomena in Small-Molecule Organic Light-Emitting Devices. *Chem. Mater.* **2004**, *16*, 4522−4532.

DOI: 10.1021/acsami.5b00839
ACS Appl. Mater. Interfaces 2015, 7, 6444−6450